Table 2 Ranges of orbit determination errors (ft) with unsupplemented eighth-degree, eighth-order (8/8) gravity model and model of μ and J_2 only ($e = 0.05$, $i = 5.0°$)

Gravity model used in fit[a]	Radial		In-track		Cross-track	
	8/8 model	μ, J_2 only	8/8 model	μ, J_2 only	8/8 model	μ, J_2 only
O	−950 to 110	−1,300 to 500	−3,300 to 6,000	−1,900 to 11,800	−2,500 to 2,700	−3,700 to 4,000
O and P_0	−88 to −48	−98 to −26	1,200 to 1,300	1,100 to 1,300	480 to 710	460 to 1,100
P	−9,800 to 1,700	−8,400 to −490	−45,000 to 53,100	−4,700 to 46,000	−31,100 to 34,300	−34,200 to 37,700
P and P_0	−140 to 25	−110 to −27	530 to 1,400	1,100 to 1,400	−60 to 1,400	400 to 1,100

[a] Letters O and P refer to "optimistic" and "pessimistic" gravity models in Table 1; P_0 = polynominal.

reasonable for Baker-Nunn cameras. For all cases considered, nominal station mislocation errors were taken at 150 ft in latitude and longitude and 25 ft in altitude.

The gravity model errors listed in Table 1 were assumed in the "perfect" 8/8 model used in the simulation. These errors appear to span the precision of our present knowledge of the terrestrial gravity field.[2,3] In Table 1, μ is the product of the universal gravitational constant and the mass of the earth, and J_n and J_{nm} are coefficients of the zonal and nonzonal harmonics, respectively, with the n subscript designating the degree and the m subscript the order.

All of the orbits analyzed in Ref. 1 had four osculating elements (semimajor axis, argument of the ascending node, argument of perigee, and time of perigee passage) in common; with the semimajor axis chosen so as to yield the near synchronous condition. Thus, these orbits were completely specified by their orbital inclinations i, and eccentricities, e. It should also be noted that those two elements serve to approximate the latitudinal and longitudinal excursions respectively; the maximum vehicular sublatitude being nearly equal to the inclination and the longitudinal excursion, $\Delta\lambda$, being closely approximated, for small to moderate eccentricities, by[4] $\Delta\lambda = 2e \sin nt$, where n is the mean motion. Thus, for near-synchronous, near-equatorial satellite orbits a maximum longitudinal excursion of approximately $\pm 2e$ rad will be encountered.

One of the orbits analyzed in Ref. 1 (therein designated as the case 3 orbit) was specified by $e = 0.05$ and $i = 5.0°$. This analysis extends that of Ref. 1 to a consideration of the orbit determination accuracy attainable when the polynomial force model is used to supplement a gravity model consisting only of μ and J_2 terms. The gravity model errors listed for μ and J_2 in Table 1 (and designated "optimistic" and "pessimistic") were used in the fit. In this case, all other coefficients in the 8/8 gravity model were set equal to zero for the orbit determination. Table 2 compares ranges of orbit determination errors throughout the 20-day data span associated with this orbit as determined by the 8/8 model with those determined by the μ and J_2 only model. For purposes of this analysis, the orbit determination error is defined as the difference between the position vector resulting from the fit, projected forward (within the 20-day data span) utilizing the same gravity model used in the fit and the perfect epoch vector utilized in the simulation projected forward to the time of interest utilizing the perfect 8/8 gavity model in the simulation.

One is struck by the ability of the polynomial representation to compensate for errors induced by even extremely truncated fitting models. In fact, as long as the polynomial force model is used as a supplement, the resulting orbit determination accuracy is insensitive to choice of base model.

References

[1] Hall, N. S. and Gersten, R. H., "A Polynomial Force Model Representation for Determining Near-Equatorial, Near-Synchronous Sattellite Orbits," *Journal of Spacecraft and Rockets*, Vol. 6, No. 4, April 1969, pp. 503–504.

[2] Kaula, W. M., "Determination of Variations in the Gravitational Field for Calculation of Orbit Perturbations," TDR 269(4922-10)-2, July 1964, Aerospace Corp., El Segundo, Calif.

[3] Kaula, W. M., "Comparison and Combination of Satellite with Other Results for Geodetic Parameters," *Second International Symposium; The Use of Artificial Satellites for Geodesy, Athens, April 1965*, Publication 431, Institute of Geophysics and Planetary Physics, Univ. of California at Los Angeles, 1965.

[4] Whittaker, E. T., *Analytical Dynamics of Particles and Rigid Bodies*, Cambridge Univ. Press, 1964, Chap. 4.

A Semiempirical Study of Pressure Oscillations in LOX Pump Inducers

C. K. Liu* and A. L. Worlund†

NASA Marshall Space Flight Center, Huntsville, Ala.

THIS analysis is concerned with the pressure oscillations in the liquid oxygen (LOX) pump inducer of the J-2 engine. A distinct frequency band exists for a certain combination of the pump inlet pressures and mixture ratios.[1] To locate this band of oscillations in a plot of inlet pressure P_i vs mixture ratio MR, a semianalytical first-order model with a retarded time mechanism is introduced. It is necessary to evaluate several constants in the formulation from the available experimental results for a certain inducer under consideration. Since the available experimental data show that the variation between the frequency ranges and inlet pressure magnitudes was approximately linear, two attempts are made to depict first-order models. One is oriented principally toward P_i, with MR appearing only as a multiplier whose influence is limited to narrowing or widening the corridor of pressure oscillations. The other model is MR-oriented.

Formulation of Analytical Model (P_i-Oriented)

It is postulated at the outset that the pressure rate of change in the inducer at any instant, t, is proportional to the net contributions from the pressure at the present instant $t = t$ and from the pressure at a previous instant $t = t - t_1$ (later t_1 is set to be C_2/f); these contributions must be appropriately augmented with respect to the nominal, P_i. In mathematical terms, it can be written

$$\frac{dP(t)}{dt} = \frac{C_3}{MR}\left[\frac{P_i - C_i}{P_0}P(t) - \frac{P_i}{P_0}P\left(t - \frac{C_2}{f}\right)\right] \quad (1)$$

where P_0 = characteristic pressure; C_1 = constant pressure term to be determined from the experimental results; $C_2/f = t_1$; C_2 = pure constant to be determined from the experimental results; f = frequency of the pressure oscillations; and C_3 = scaling factor ($\sec^{-1}$). This equation is solved by Laplace

Received September 18, 1969.

* Consultant; also Professor of Mechanical Engineering, Department of Mechanical Systems Engineering, University of Alabama, Ala.

† Chief, Fluid Mechanics and Dynamics Branch, Astronautics Laboratory, Science and Engineering Directorate.

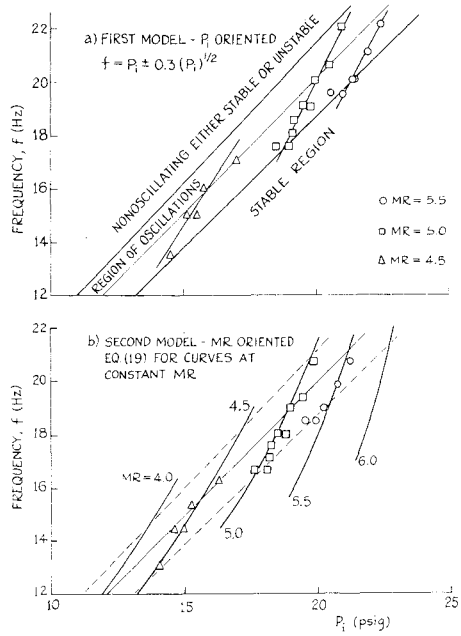

Fig. 1 a) Frequency-inlet pressure relations in region of oscillations; b) frequency-inlet pressure relations for oscillation-prone pump operations for various mixture ratios.

transform techniques using the well-known formula[2]

$$e^{-AS}\, p(S) = \int_0^\infty e^{-St} P(t - A)dt \tag{2}$$

where S is the transformation parameter. As a result, Eq. (1) becomes

$$(MR/C_3)[S\, p(S) - P(0)] = (P_i - C_1)p(S) - P_i e^{-C_2 S/f}\, p(S) \tag{3}$$

Solving for $p(S)$ from Eq. (2) gives

$$p(S) = \frac{(MR/C_3)P(0)}{SMR/C_3 + C_1 - P_i + P_i e^{-C_2 S/f}} \tag{4}$$

With a view to inverting $p(S)$ from the S domain to the physical t domain, one naturally seeks the zeros of the denominator of the right side of Eq. (4). This can be accomplished in general by graphical means.

Set

$$g_2(S) = \frac{P_i - C_1 - (MR/C_3)S}{P_i} = e^{-C_2 S/f} = g_1(S) \tag{5}$$

Superimposing the plots $g_1(S)$ and $g_2(S)$ vs S on the same graph, two intersections are obtained between the straight lines $g_2(S)$ and the exponential curve $g_1(S)$. It can be shown that the presence of intersections on the positive S axis signifies instability of $P(t)$ for a given combination of P_{i1} and f_1; whereas intersections on the negative S axis indicate stability of $P(t)$ for a similar given combination of P_{i2} and f_1. The process is then repeated for all combinations of P_i and f, thus determining the stable and unstable regions of $P(t)$ in a $P_i - f$ plane.

Unquestionably, this process of solving Eq. (5) graphically is time consuming. Since an excessive amount of labor is unwarranted at this stage of analysis, an alternative is to replace the exponential term in Eq. (5) with the first three terms of its equivalent approximation expansion series, resulting in

$$\frac{MR}{C_3} S + C_1 - P_i + P_i \left(1 - \frac{C_2}{f} S + \frac{C_2^2}{2!\, f^2} S^2 - \ldots\right) = 0 \tag{6}$$

Simplifying

$$(C_2^2 P_i/2f^2)S^2 + (MR/C_3 - C_2 P_i/f)S + C_1 = 0 \tag{7}$$

where

$$S = \frac{f^2}{C_2^2 P_i}\left\{\frac{C_2 P_i}{f} - \frac{MR}{C_3} \pm \left[\frac{(MR)^2}{C_3^2} - \frac{2P_i MRC_2}{fC_3} + \frac{C_2^2 P_i^2}{f^2} - \frac{2C_i C_2^2 P_i}{f^2}\right]^{1/2}\right\} \tag{8}$$

The region of oscillations is bordered by the curve on which the S roots are equal. In other words, the region of oscillations is outlined by all the combinations of f and P_i for which the straight lines $g_2(S)$ are tangent to the exponential curve $g_1(S)$. The points of tangency give equal roots of S. This requires that the contents of the radical in Eq. (8) vanish. Hence,

$$(MR/C_3)^2 f^2 - (2C_2 MR/C_3)P_i f + (C_2^2 P_i^2 - 2C_1 C_2^2 P_i) = 0 \tag{9}$$

where

$$f = (C_2 C_3/MR)[P_i \pm (2C_1 P_i)^{1/2}] \tag{10}$$

Thus f is bracketed by two curves represented by the $\pm$ term; and the region between these two limiting curves corresponds to pump operations which are oscillation-prone; it spreads approximately equally on both sides of a 45° line emanating from the origin (Fig. 1a). As the pump inlet pressure increases, the region widens slightly, indicating clearly its dependence on P_i and MR. Similarly, C_1, C_2, and C_3 may be functions of MR. For simplicity, it is assumed that C_i is independent of MR while the remaining constant $(C_2 C_3)$, considered as one entity, is assumed to be dependent on MR.

Using the data depicted in Fig. 1, $C_1 = 0.045$ lbf/ft², and $C_2 C_3/MR = 1$ ft²/lbf-sec. Equation (9) now takes the form

$$f = P_i \pm 0.3\ (P_i)^{1/2} \tag{11}$$

Equation (11) gives numerically correct predictions if P_i is given in psig and f in Hz.

The results in Fig. 1a seem to indicate that MR, as it is featured in the model, exerts little or no influence on the location and size of the instable region in a $f - P_i$ plane. At most, it can either narrow or widen the corridor of oscillations.

Second Analytical Model (MR Oriented)

With a view toward investigation of the effect of MR on the frequency of oscillations, the following equation may be written:

$$\frac{dP(t)}{dt} = \frac{MR - C_1}{M_0} P(t) - \frac{P_i}{P_0} fP\left(t - \frac{C_2}{f}\right) \tag{12}$$

in which most of the symbols have the same meaning as in the first model and M_0 is a characteristic time. Using the Laplace transform, we obtain, after transposition,

$$p(S) = \frac{P(0)}{S - (MR - C_1)/M_0 + (P_i/P_0)fe^{-C_2 S/f}} \tag{13}$$

Replacing $e^{-C_2 S/f}$ with the first three terms of its series expansion, and letting $\xi \equiv C_2 P_i/P_0$, we obtain

$$S^2 + \frac{2f}{\xi C_2}(1 - \xi)\, S + \frac{2f^2}{C_2^2} - \frac{2f}{\xi C_2}\frac{MR - C_1}{M_0} = 0 \tag{14}$$

where

$$S = \frac{f}{C_2\xi}\left\{\xi - 1 \pm \left[(1-\xi)^2 - 2\xi^2 + \frac{2\xi C_2}{f}\frac{MR - C_1}{M_0}\right]^{1/2}\right\} \quad (15)$$

The condition for S to have equal roots is the vanishing of the radical in Eq. (15); thus,

$$f = 2C_2\frac{C_1 - MR}{M_0}\frac{\xi}{2 - (1+\xi)^2} \quad (16)$$

in which the constants C_2/P_0, $C_1C_2^2/P_0M_0$, and C_2^2/P_0M_0 must be determined from the available experimental data for the pump inducer under consideration. When these constants are properly determined, Eq. (16) becomes

$$f = (1.900 - 0.279\,MR)\,P_i/[2 - (1 + 0.00225\,MRP_i)^2] \quad (17)$$

Assigning values of 4.0, 4.5, 5.0, 5.5, and 6.0 to MR, five curves, f vs P_i, may be plotted as shown in Fig. 1b. The experimental data for MR = 4.5, 5.0, and 5.5 are also shown in Fig. 1b.

Conclusions

The analysis contained herein employs a first-order mathematical model, the mechanism of which is dependent on the experimental data observed on the *J*-2 LOX pump inducer under consideration. This semiempirical approach to the present study is deemed necessary, because a general study of a problem of this kind would entail investigations in at least the following disciplines of physical science: gas dynamics, bubble dynamics, cryogenics, vibration, hydrofoil dynamics with full or partial cavitation, etc., and with coupling among various thermal, hydrodynamic, and fluid flow effects. Such a study would be extremely time consuming, if not impossible. On the other hand, guided by the experimental evidence as to the occurrence of instability in a frequency, f, vs pump inlet pressure, P_i, plot, with the mixture ratio as a parametric constant, a model can be devised having a retarded time (αf^{-1}) for the present study. The result is an approximate relationship among the principal variables P_i, f, and MR, which outlines the region of instability or the region of oscillation-prone pump operations.

Two such model studies were undertaken in this report: the first is pump inlet-pressure oriented, the second is mixture ratio oriented. When the resulting curves from both model studies were superimposed on the same frequency vs inlet pressure plot, areas of instability or regions of pressure oscillations corresponding to different values of mixture ratios are clearly indicated. With such a plot available, predictions for occurrence of oscillations in some heretofore unsuspected areas can be made. To rephrase it, some undesirable frequency (mixture ratio combinations which would give rise to pressure oscillations in the pump inducer) can be forecast.

Some mathematical expediency is exercised in solving for the roots of Eq. (5). The resultant saving of computational work can be easily appreciated. However, as a consequence of this approximation, extrapolation beyond P_i = 25 psig (first model) and exceeding MR = 6.0 (second model) is not suggested.

The mixture ratio is a function of the N (rpm) and the flow coefficient (Q/N) of the pump, where Q is the volumetric flow rate. With the previously derived marginal stability relationships among f, P_i, and MR, one can extend the usefulness of the formulation by relating the frequency of oscillations to the flow coefficient (angle of attack) and the absolute speed of the pump.

References

[1] Gross, L. A., "J-2 Engine Test Report," March 1969, NASA.
[2] Churchill, R. V., *Operational Mathematics*, McGraw-Hill, New York, 1958.

Vehicle Flight Scaling with Aerodynamic Flow Hysteresis

PETER JAFFE*
Jet Propulsion Laboratory, Pasadena, Calif.

Nomenclature

A	=	cross-sectional area of body
C_D	=	drag coefficient
C_m	=	pitching moment coefficient
C_{m_α}	=	pitching moment coefficient slope
$C_{m_q} + C_{m_{\dot\alpha}}$	=	dynamic stability coefficient
C_{L_α}	=	lift coefficient slope
d	=	diameter of body
I	=	transverse moment-of-inertia
m	=	mass of body
α	=	angle of attack
$\delta\alpha$	=	angle-of-attack decay in half cycle
ρ	=	atmospheric density
Ω	=	distance frequency of oscillation, rad/ft of travel

CERTAIN aerodynamic configurations, particularly those with flares, are susceptible to flowfield hysteresis as a result of the oscillatory motion they experience in flight. The consequence of this hysteresis is that the static aerodynamic coefficients are no longer single-valued functions of the angle of attack. Since most free-flight analyses[1,2] assume single-valued functions, there is a question about the correctness of using the coefficients obtained from a test to predict the motion of the actual vehicle when hysteresis is present.

This Note will consider the simplest case: a vehicle oscillating in a plane and experiencing a pitching moment hysteresis. The pitching moment history, as the vehicle oscillates from zero angle of attack to its amplitude α_0 and then back to zero again, is shown in Fig. 1. As a result of the hysteresis, the energy associated with each half of the motion is different.

A derivation of the dimensionless angle-of-attack decay $\delta\alpha/\alpha_0$ for this case, using an energy balance method is given in Ref. 3. The lift-slope and drag coefficients are assumed constant and the hysteresis is assumed superimposed on a

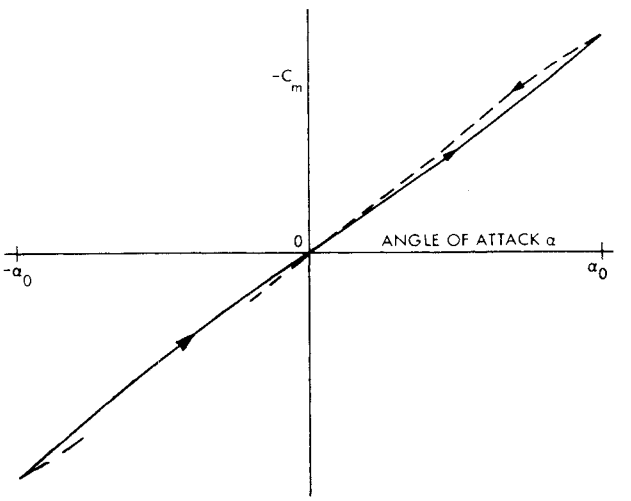

Fig. 1 Pitching moment coefficient with hysteresis.

Received September 17, 1969. This paper presents the results of one phase of research carried out at the Jet Propulsion Laboratory, California Institute of Technology, under Contract NAS 7-100, sponsored by NASA.

* Member of the Technical Staff. Member AIAA.